Master's Thesis

Multi-dimensional Carbon Composites for Flexible Supercapacitors

Cheolwon An

Department of Chemical Engineering

(Chemical engineering)

Graduate School of UNIST

2019

Multi-dimensional Carbon Composites for Flexible Supercapacitors

Cheolwon An

Department of Chemical Engineering
(Chemical Engineering)

Graduate School of UNIST

Multi-dimensional Carbon Composites for Flexible Supercapacitors

A thesis/dissertation
submitted to the Graduate School of UNIST
in partial fulfillment of the
requirements for the degree of
Master of Science

Cheolwon An

12. 5. 2018

Approved by

Advisor
Ji-Hyun Jang

Multi-dimensional Carbon composites for Flexible supercapacitors

Cheolwon An

This certifies that the thesis/dissertation of Cheolwon An is approved.

12. 05. 2018

Signature

Advisor: Ji-Hyun Jang

Signature

Hyun-Kon Song

Signature

Jongnam Park

Table of Contents

List of Figures **7**

Abstract **9**

Chapter 1. Review of supercapacitors **10**

1.1 introduction **10**

1.2 Carbon materials in EDLC **13**

1.2.1 Carbon nanotubes (CNT)s in EDLCs **16**

1.2.2 Graphene in EDLCs **16**

1.2.3 Mesoporous carbon in EDLCs **17**

Chapter 2. Multi-dimensional carbon composites for flexible supercapacitors **18**

2.1 Introduction **18**

2.2 Experimental section **20**

2.2.1 Materials **20**

2.2.2 Fabrication of 3D-Gn **20**

2.2.3 Preparation of electrode and cells **22**

2.2.4 Characterization **22**

2.2.5 Electrochemical quartz crystal microbalance (EQCM) **22**

2.3 Results and discussion **23**

2.3.1 Fabrication of multi-dimensional carbon composite **23**

2.3.2 Capacitance **31**

2.3.3 Electrochemical analysis **34**

2.3.4 Flexibility **38**

2.4 Conclusion **41**

Reference **42**

List of Figures

Figure 1. 1. Schematic illustration for (a) an EDLC, (b) a pseudocapacitor **11**

Figure 1. 2. Ragone plot of energy versus power density for various ESS electronics **12**

Figure 1. 3. Various carbon materials for EDLCs **14**

Figure 1. 4. Electrochemical performances. (a) Cyclic voltammetry and (b) galvanostatic charge discharge profiles of carbon materials[55]. **15**

Figure 2.1. Schematic illustration of (3*+2+1)D carbon composites. **19**

Figure 2.2. Schematic illustration of fabrication process for 3D-Gn **21**

Figure 2.3. Morphology of 3D-Gn*(a-d). **24**

Figure 2.4. Activated 3D-Gn (3D-Gn*) by CO_2 activation. Nitrogen adsorption/desorption isotherms (a). Pore size distribution (b). **25**

Figure 2.5. Morphology of 2D-Gn (a-c) and 1D-CNT (d-f). **26**

Figure 2.6. Characterization of 3D-Gn*, 2D-Gn and 1D-CNT. Nitrogen adsorption/desorption isotherm (a). Surface area calculated by Brunauer, Emmett and Teller equation (b). XRD patterns (c). Raman spectra (d).. ..... **27**

Figure 2.7. Morphology of (3*+2+1)D carbon composites. **28**

Figure 2.8. Electric conductivities (σ) measured by 4-point probe method of 1D, (2+1)D, (3*+1)D and (3*+2+1)D carbon composites. **30**

Figure 2.9. Capacitances. Cyclic voltammograms at 20 mV s^{-1} (**a**) and 200 mV s^{-1} (**d**). Capacitance calculated from **a** and **c**. Each capacitance of carbon composites calculated from **b** and **d**. **32**

Figure 2.10. Capacitance of (3*+2+1)D versus (3*+1)D. Cyclic voltammograms. (a and b), Capacitance according to scan rates.(c) Galvanostatic charge/discharge profile. (d and e) Capacitance according to current densities (f). Capacitance retention along repeated 100,000 cycles of charging and discharging at 10 A g^{-1}. (g) Energy density versus power density in Ragone plot. **33**

Figure 2.11. Electric double layer formation investigated by electrochemical quartz microbalance. Frequency changes (Δf) during voltage sweep at 10 mVs^{-1} (a and b). Mass differences (Δm) between (3*+2+1)D and (2+1)D or between (3*+1)D and 1D (c). **35**

Figure 2.12 Electrochemical impedance spectra (**a**). Experimental data were fitted by transmission line model with pore size distribution (TLM-PSD). Pore length of 3D-Gn* in (3*+2+1)D and (3*+1)D calculated from TLM-PSD (**b**). **37**

Figure 2.13 Flexibility of (3*+2+1)D or (3*+1)D on polymer substrates versus 3D*|Al. Mass loss on repeated crumpling (a). Resistance developed along repeated folding (c to h). Top views around folding lines in SEM images at 0, 500 and 1000 times folding: (3*+2+1)D on the

left versus (3*+1)right. 39

Figure 2.14 Folded supercapacitors. CVs of flexible supercapacitors based on a symmetric (3*+2+1)D electrode configuration on bending at 0º, 90 º and 180 (b-e). 40

ABSTRACT

In recent year, Researches on flexible energy storage devices used in various fields such as wearable devices, roll-up displays, electronic sensors, and foldable mobile phones have been attracted. Rechargeable batteries such as lithium ion batteries (LIBs) and supercapacitors or electric double layer capacitors (EDLCs) are representative devices that can be applied to flexible energy storage devices. But they have differences in applications. Supercapacitors have been developed for high power applications due to their high-power density, rapid charge/discharging, and longer operation lifetime that LIBs. On the other hands, LIBs have higher energy densities than them of supercapacitors and it used as high energy applications. Flexible supercapacitors and batteries require various properties such as light weight, good electrochemical performances, and high power/energy density. In particular, good mechanical durability, even in situations where it is folded and crumped, is a key component in addition to having a high power/energy density.

At this paper, we designed carbon electrode to guarantee flexibility of symmetric electric double layer capacitors by using three different dimensional carbon materials. These carbon materials were combined to gain the flexibility as well as high performances. Three-dimensional graphene (3D-Gn*) is highly capacitive but poorly-conductive and it is used as a platform for electric double layer formation. One-dimensional carbon nanotube (1D-CNT) plays a role as an electrically conductive highway. And finally, two-dimensional graphene (2D-Gn) makes them facilitate electron communications between 3D-Gn* and 1D-CNT. And we used a flexible polymer substrate that is Polyethylene terephthalate micro fiber (PET MF) mat having polyacrylonitrile nanowire (PAN-NW) back-layer on a face (PET-MF/PAN-NW). In terms of mechanical properties, the 1D-CNT is used to reinforce the active composite layer by anchoring between the 3D-Gn* that was active material and flexible polymer matrix (PET-MF/PAN-NW). Consequently, the symmetric EDLC used multi-dimensional carbon composites anchored to flexible substrates was operated at 3V, ensuring high energy densities even under repetitive mechanical stress conditions.

Chapter 1. Review of supercapacitors.

1.1 Introduction

The increasing cost of fossil fuel and environmental pollutions such as global warming have caused attention of friendly energy-generation and storage technologies. In particular, many people are interested in researches on energy storage devices such as batteries and electrochemical supercapacitors. Among them, electrochemical supercapacitors have attracted significant attention due to their high power density and long life cycle[1,2].

The electrochemical supercapacitors are composed of two electrodes and separator that positioned between electrodes[3,4]. And they can be divided into two types depending on the method of charge storage. One is electric double-layer capacitors. For electric double-layer capacitors, charge storage occurs at the interfaces between the electrodes and electrolyte by using electrodes that have ideally polarizable properties[5] **(Fig. 1.1a)**. When one electrode is polarized to have a negative charge and the other electrode is polarized to have a positive charge through current collector, the cations in the electrolyte migrate to the negative electrode to form an electric double layer, and the anions form an electric double layer on the positive electrode for charging. Thus, they usually use electrodes that have high electronic conductivity and surface areas. The other is pseudo-capacitors that store charge by reversible and fast faradaic redox reactions[6] **(Fig. 1.1b)**.

As illustrated **Figure 1.2**, the supercapacitors have higher power densities than batteries and fuel cells, but they have lower energy densities. However, they can store more electricity than conventional condensers. The supercapacitors have high power densities because it can charge and discharge with a very large current density. This is because it is physically charged and discharged on the electrode surface or the charge transfer reactions proceed only on the electrode surface, so that it is not necessary that the ions diffuse into the bulk of the active material on the electrode like the batteries. Therefore, the degradation of electrode is not so severe that it can be used semi-permanently. But, since the charge is stored only on the surface of the electrode, the energy density is small due to the small storage capacity. On the contrary, in the case of the battery, the faradaic reactions proceed inside of the active materials on the electrode, so the electric storage capacity is large and energy density is also large. However, the power densities are lower than that of supercapacitors because diffusion of ions into active materials is slow[8].

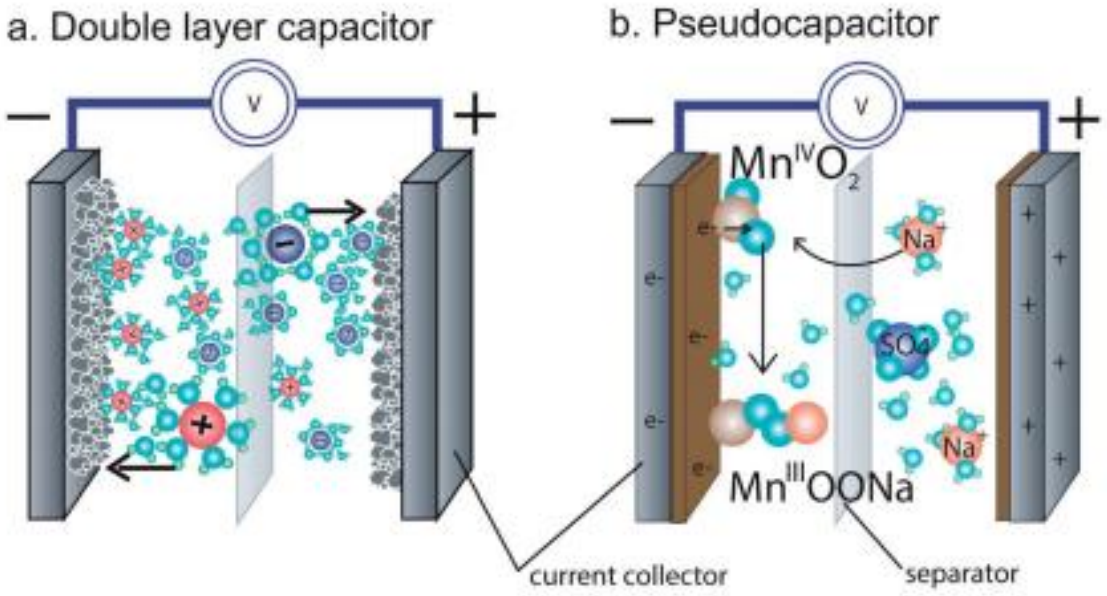

Figure 1.1 Schematic illustration for (a) an EDLC, (b) a pseudocapacitor[9].

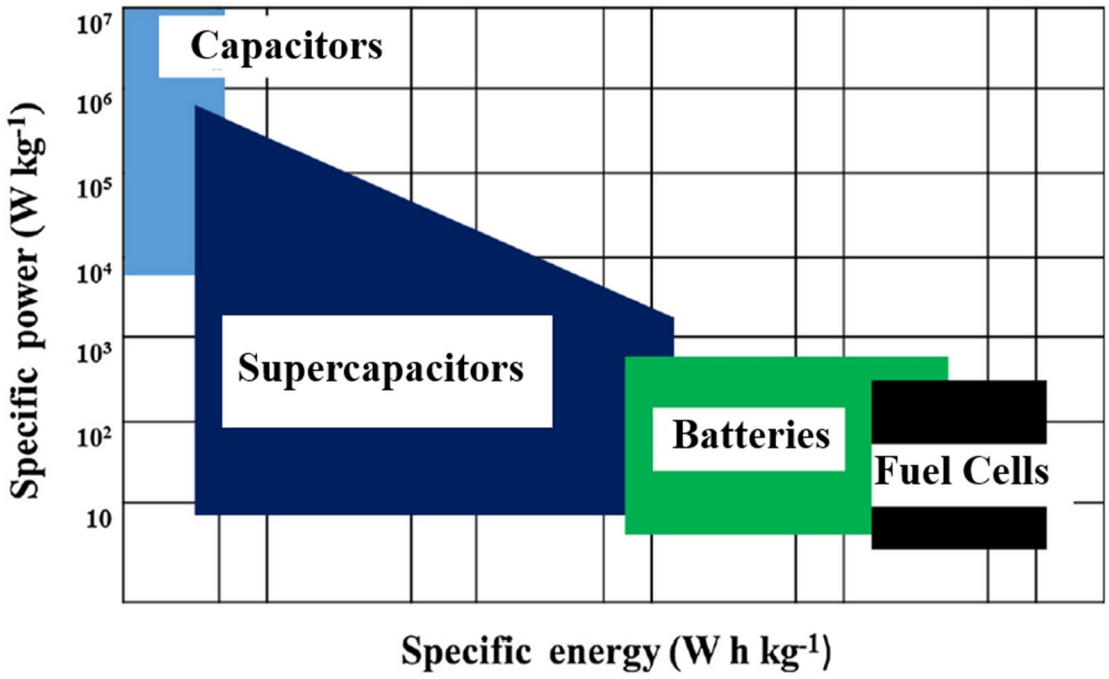

Figure 1. 2. Ragone plot of energy versus power density for various ESS electronics[10].

1.2 Carbon materials in EDLC

Carbon materials are used to fabricate supercapacitors as electrode materials in various forms[8] **(Fig. 1.3)**. Due to the properties such as high surface area, low cost, availability, and established electrode production technologies, they usually used as electrode materials in supercapacitors. As shown in **Figure 1.4a**, rectangular shape of cyclic voltammetry curves of carbon materials show that the carbon materials are appropriate materials for supercapacitors. Also, carbon materials show triangular symmetrical distribution in galvanostatic charge-discharge profile (**Fig. 1.4b**)[10]. It indicates that they have good capacitive properties for supercapacitors. Normally, the electrochemical double layer is formed at the interface between the electrode and electrolyte. So, the capacitance depends on the surface area of carbon materials that can be accumulate to electrolyte ions. There are many factors that influence their electrochemical performance such as specific surface area, pore-size distribution, pore shape and structure, electrical conductivity, and surface functionality. Among these, specific surface area and pore-size distributions are very important factors influencing the performance of carbon materials. Example of carbon materials used as electrodes are carbon nanotubes, mesoporous carbon and graphene etc[11-13].

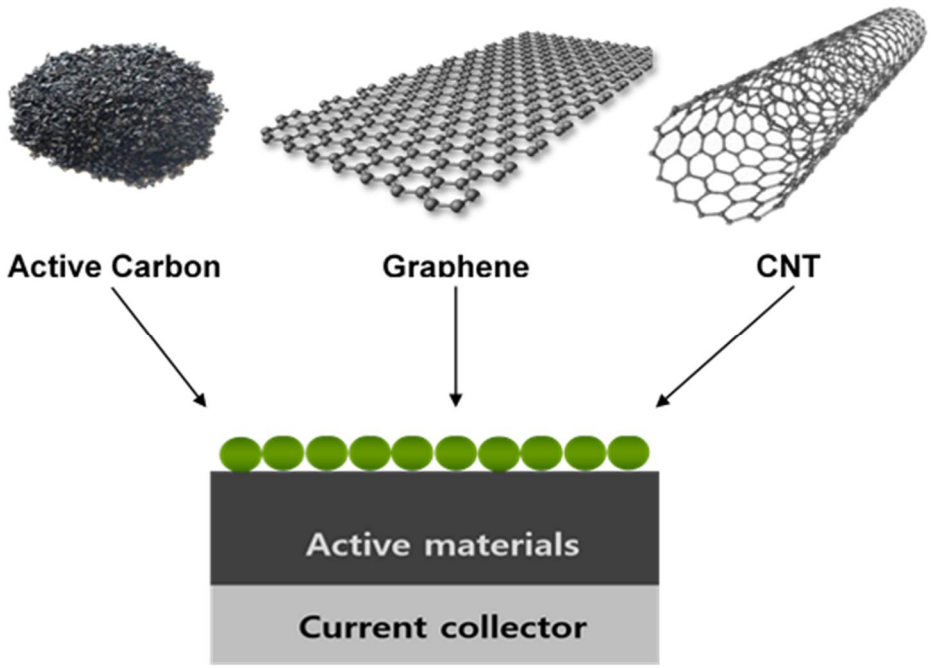

Figure 1.3. Various carbon materials for EDLCs

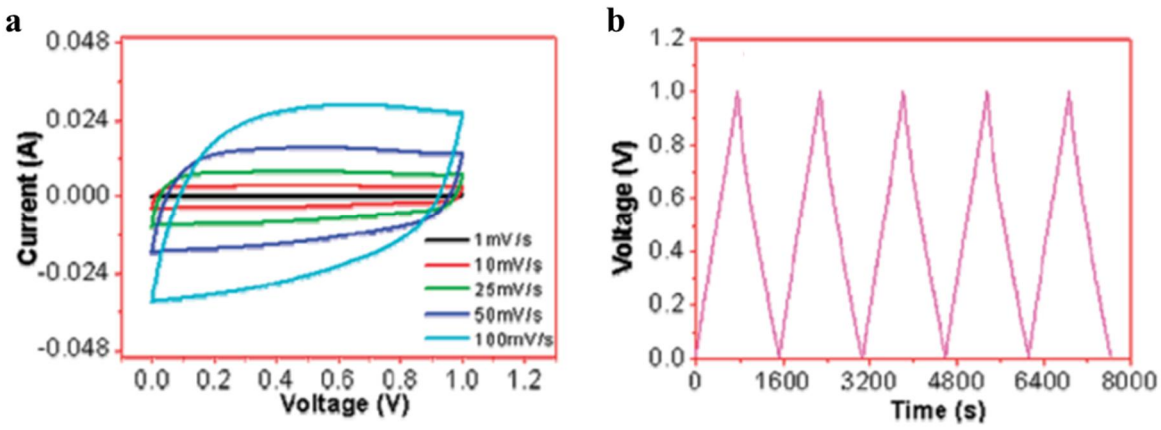

Figure1.4. Electrochemical performances. (a) Cyclic voltammetry and (b) galvanostatic charge/discharge profiles of carbon materials[55].

1.2.1 Carbon nanotubes (CNTs) in EDLCs

CNTs have important material properties that can be very useful as supercapacitor materials. Among these, the most important properties of CNTs are their electronic, optical, chemical, and mechanical characteristics. They exhibit superior electronic conductivity and good mechanical properties[14-16]. CNTs are produced through the catalytic decomposition of some hydrocarbons, and careful manipulation of other parameters can generate nanostructures of various conformation and control their crystalline structures[17]. CNTs are unlike any other carbon-based electrodes, and they have interconnected mesopores, which allows for a continuous charge distribution that can use most of the surface areas. This is why the CNT-based electrodes can have a higher capacitance even though the activated carbon electrode have a larger surface area. Also, since electrolyte ions can diffuse into the mesoporous nature of CNT networks, CNTs have lower equivalent series resistance than the activated carbon and a higher maximum usable power[18].

1.2.2 Graphene in EDLCs

Graphene is a one atom thick layer 2D structure composed of all-sp2-hybridized carbons and it has unique properties of high electrical conductivity, chemical stability and highly surface area (up to $2675 m^2 g^{-1}$)[19,20]. Due to these properties, recently, graphene or graphene-based materials more attractive for electrochemical energy storage such as Li-ion batteries, fuel cell and supercapacitors. Especially, It has been proposed that graphene can be used as a material for supercapacitors, because it doesn't depend on the distribution of pores at solid state when graphene is used as electrode materials of supercapacitors. it can achieve a capacitance of up to 550F/g when the entire specific surface area is fully utilized[21]. Another advantage of using graphene as electrode materials is that the major surfaces of graphene sheet are exterior and easily accessible by electrolyte. For energy storage application, there are many other methods for production of graphene such as chemical vapor deposition (CVD), mechanical cleavage of graphite, chemical exfoliation of graphite in organic solvent, unzipping of CNTs and intercalation method[22-24]. Among these, graphene prepared by CVD has good properties which are large crystal domains, monolayer structure and less defect. It can improve carrier mobility in electronic applications.

However, the actual capacitive behavior of pure graphene may be lower than expected due to the agglomeration that is it tends to restack to graphite. Therefore, to improve the overall electrochemical performance of graphene or graphene-based materials, the research is needed to find a suitable method.

1.2.3 Mesoporous carbon in EDLCs

Activated carbons use as electrode materials of supercapacitors due to its large surface area and good electrical properties. Activated carbons have various physiochemical properties with large surface areas of up to 3000 m^2 g^{-1} depending on the activation methods and the carbon precursor used. Activated carbons have porous structures that consist of micropores, mesopores and macropores. However, randomly connected micropores in low effective specific areas are hindered their advantages. It makes electrolyte ions difficult to access[25]. Mesoporous carbon that have larger pore diameter (2-50nm) is useful to supercapacitor electrode due to high specific surface area, fast ion-transport pathway, high power density and overall supercapacitance performance[26]. As an example, mesoporous carbon by carbonization of poly(vinyl alcohol) mixture showed a specific capacitance of 180 F g^{-1} in aqueous H2SO4 electrolyte. However, since the energy and power density of mesoporous carbon electrodes and volumetric specific capacitances can be affected by the mesoporous size and content, it is important that carbon materials contains appropriate mesopores and micropores for effective electrochemical energy storage[27,28].

There are many researches on the mesoporous carbon with various size and shape of pores. And it can controlled via various synthetic techniques[29]. Li W et al prepared ordered mesoporous carbon with homogeneously distributed pores of regular size. It can help charge transport and storage, and it shows improved capacitance and rate capability[29]. Also, by introducing micropores, mesoporous carbons can improve their specific capacitance. One of the methods that introduced micropores is activation with CO_2. Xia at al. prepared activated carbon with well-balanced population of micropores and mesopores by CO_2 activation at 950ºC. It can help improve the specific capacitance up to 223F g^{-1} from 115 F g^{-1} in 6M KOH and it has a high specific surface area (2749m^2 g^{-1}) [30].

Chapter 2. Multi-dimensional carbon composite for flexible supercapacitors.

2.1 Introduction

The researches on flexible energy storage are important to development of wearable devices and folding mobile phones[33-40]. Flexible supercapacitors or EDLCs are suitable for high power applications[41]. The flexibility can be given through electrode structure design, and mechanical properties can also be guaranteed[42]. Flexible substrates such as carbon cloth, graphene and polymer cloth helped to ensure this flexibility[43-45]. Nano-threads such as 1D-CNT can be anchored to flexible substrates, providing mechanical properties and electrical properties[46]. Therefore, it is important for flexible supercapacitors to ensure electrical conductivity to improve flexibility while maintaining energy storage performance.

Porous structure of 3D-Gn have high surface area to ensure high capacitance but low electron conductivity. In the case of 2D-Gn, it is advantageous from the viewpoint of flexibility, but there is a problem that the capacitance can be reduced due to the problem of restacking[47-50].

In this work, a (3*+2+1)D composite electrode without a binder was presented for flexible supercapacitors **(Fig. 2.1)**. 3D-Gn*s guaranteed high capacitance as active materials and 1D-CNT had active material fixed by anchoring on a polymer substrate. 2D-Gn is also used to compensate contact resistance.

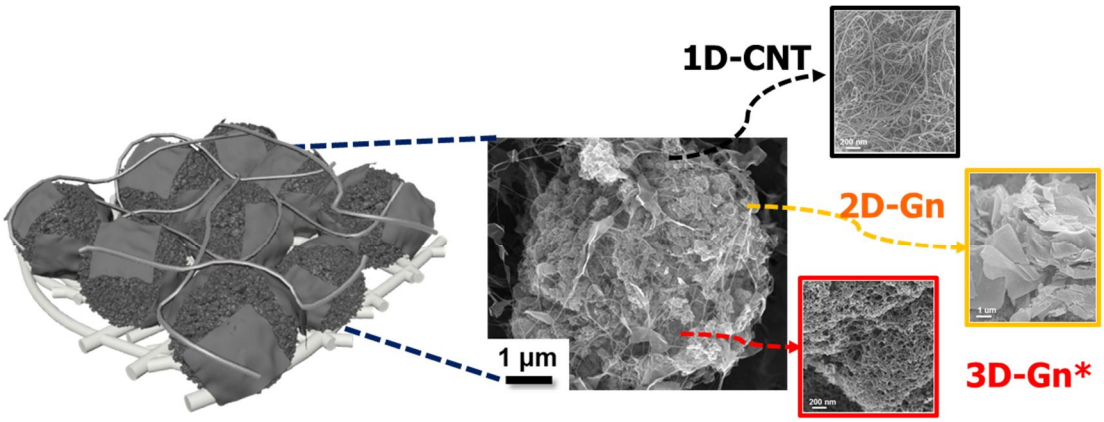

Figure 2.1. Schematic illustration of (3*+2+1)D carbon composites.

2.2 Experimental section

2.2.1 Materials

Fumed silica (size of 2-300nm), Polyvinylpyrrolidone(PVP), and Iron(III) chloride hexahydrate (FeCl3·6H2O) were purchased from Sigma-Aldrich. Single-walled Carbon nanotube (SWCNT) dispersed in water was purchased from KH science. And graphene nano-platelet grade C (xGnP) was purchased from XG science.

2.2.2 Fabrication of 3D-Gn

3D-Gn was prepared by calcination of carbon precursor mixture in a hard template in the presence of a catalyst for graphitization. The detailed processes of preparation of 3D-Gn are as follows. Firstly, 5g PVP and 17.5g $FeCl^{3}$·6H2O were dispersed in 45ml D.I water. And this aqueous solution pour into 9g fumed silica. The mixture was dried at room temperature under vacuum. And then dried mixture pyrolyzed at 900'c in continuous flow of H2/Ar at 100/1000cc min^{-1}. Ramping rate of temperature is 15'c/min to 900'c. Fe ions (III) are reduced to Fe metal and Fe species are cover the surface of SiO2 particle. PVP is decomposed and diffused into the reduced Fe species. The resultant powders were etched by using 5 wt. % HF/HCl solution in order to remove silica and iron species for 24h. Finally, the etched powders washed several times and 3D-Gn was prepared **(Fig. 2.2)**.

To achieve large specific surface area, the 3D-Gn was activated by CO2. At 900'C, 3D-Gn was activated for 15min under Ar/CO2 condition at 100/150 cc min-1. And cooling process was conducted under Ar condition. The activated resultant powder is called 3D-Gn*.

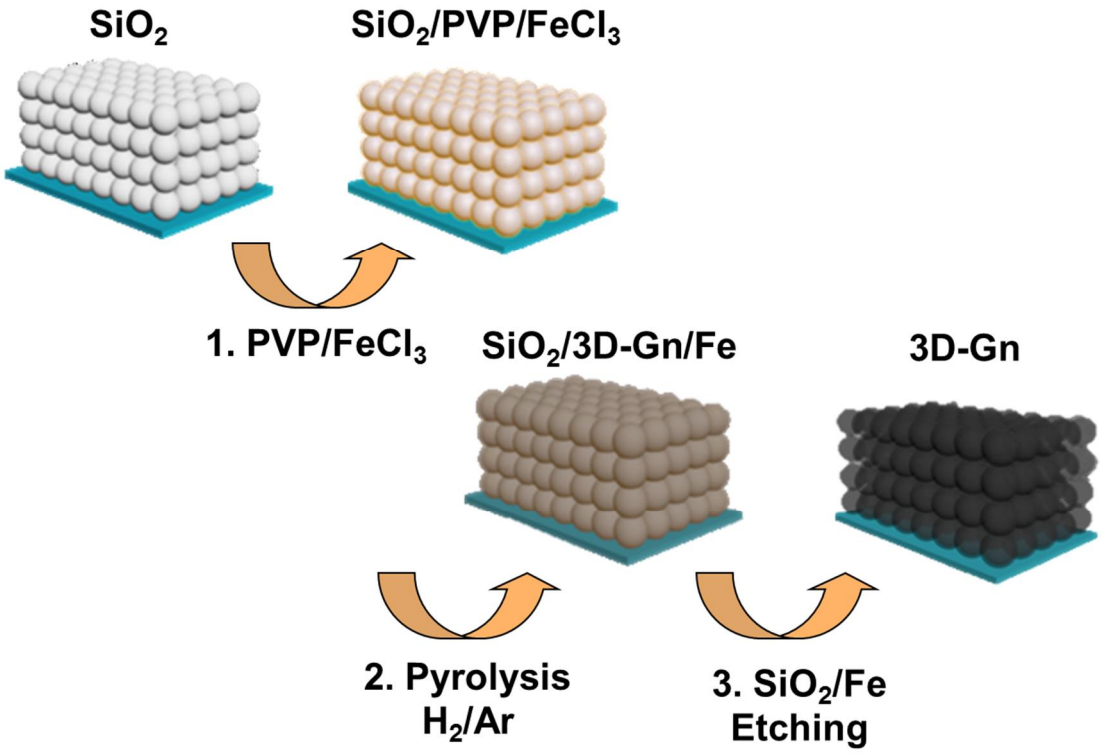

Figure 2.2. Schematic illustration of fabrication process for 3D-Gn.

2.2.3 Electrode and cells.

The (3*+2+1)D electrode was fabricated by vacuum-filtration of an aqueous solution of 1mg 3D-Gn*, 0.3mg 2D-Gn and 1.5ml 0.1wt% CNT solution on PET-MF/PAN-NW. (3*+1)D electrode was fabricated without 2D-Gn by described above method. Symmetric supercapacitor coin cells were assembled by sandwiching a commercial fiber membrane between two carbon composite electrodes on flexible substrate. And electrolyte used 1M $TEABF_4$ in acetonitrile.

2.2.4 Characterization

A scanning electron microscope (S-4800, Hitach, 10kV) and a transmission electron microscope (JEM-2100, JEOL, 200 kV) was used for observing morphological images. Surface area and pore size distribution were measured by using nitrogen physisorption analyzer (ASAP2420, Micromeritics Instruments). Raman spectroscopy (alpha300R, WITec) and X-rap photoelectron spectroscopy (K-alpha, ThermoFisher) were used. Potentiostat(VSP-300, Biologic) was used for measuring cyclic voltammograms and chronopotentiometric curves.

2.2.5 Electrochemical quartz crystal microbalance (EQCM)

Active materials were loaded on gold-coated quartz crystal resonators and binder used Nafion. The active-material loading resonator, Platinum plate and Ag/Ag+ was used as a working electrode, a counter electrode and reference electrode, respectively. Mass of the ions participating in forming electric double layer on electrode (m) were calculated by multifying frequency change (Δf) by a sensitivity factor of 900 kHz resonator (1.069 ng Hz^{-1}). Electrochemically available surface area (A_{EQCM}) can calculated from mass difference (Δm) that is the cation mass difference of ions participated in forming electric double layer (m) between (3*+2+1) D and (2+1) D or (3*+1)D and 1D with the assumption that cation monolayer was formed on the surface of 3D-Gn*[56-57]. :

$$A_{EQCM} = \frac{|\Delta m|}{MW_{TEA^+}} N_{Avogadro} \pi R^2 / M_{3D}$$

where $N_{Avogadro}$ = Avogadro number; M_{3D} = loading mass of 3D-Gn* on resonator = 3.33 μg; MW_{TEA^+} = molecular weight of TEA^+ = 130.25g/ mol ; R = radius of TEA^+ = 0.68 nm[27].

2.3 Results and Discussions

2.3.1 Fabrication of multi-dimensional carbon composite

The 3D-Gn was fabricated by calcination of polyvinylpyrrolidone (PVP) and FeCl3 infiltrated in silica particles and then removing the silica template and FeCl3 by etching. The PVP, FeCl3 and silica particle used as carbon precursor, graphitization catalysts and hard template, respectively **(Fig. 2.2)**. The 3D-Gn have hierarchical pore structure that involving micropores, mesopores, and macropores. **(Fig. 2.3 a-d).** Also, its surface area is 1200 m^2 g^{-1} and pore volume is 2.0 cm^3 g^{-1}. 3D-Gn* is activated 3D-Gn by CO_2. It showed that increased surface area (1600m^2 g^{-1}) and pore volume (2.2 cm^3 g^{-1}) **(Fig. 2.4)**. The 2D-Gn showed higher crystallinity than 3D-Gn and had the advantages of high electron mobility along the surface of 2D-Gn. And 1D-CNT was used as an electron pathway and anchor to individual materials **(Fig. 2.5, and 2.6)**. The surface area of 2D-Gn and 1D-CNT is 600 m^2 g^{-1} and 12 m^2 g^{-1}, respectively and it is smaller than that of the 3D-Gn* **(Fig. 2.6)**.

The (3*+2+1)D composite electrodes were fabricated by filtering a aqueous solution that dispersed 3D-Gn*, 2D-Gn and 1D-CNT on the PET-MF/PAN-MF membrane **(Fig. 2.7)**. Since the PAN-MF layer has a smaller pore than the PET-MF layer, the 1D-CNT penetrated the PET-MF layer but not the PAN-MF layer. 3D-Gn* particles and 2D-Gn leaflets are anchored by 1D-CNT, and 2D-Gn leaflets promoted electron conduction between 3D-Gn*s and between 3D-Gn* and 1D-CNT. This (3*+2+1)D carbon composite electrode showed a strong integrity and showed that the individual material did not fall off even when the electrode was folded.

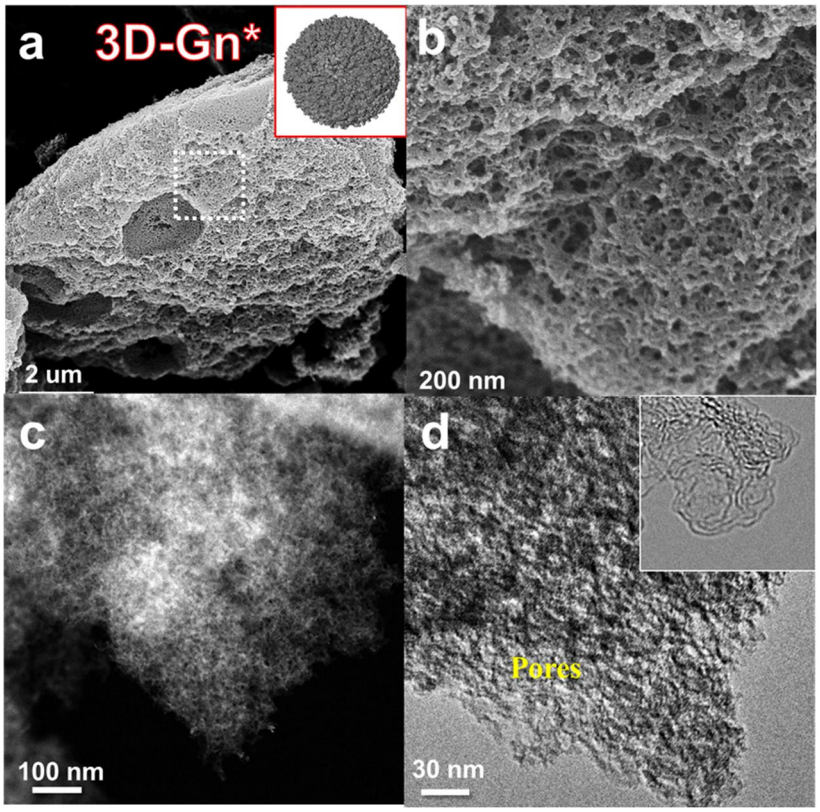

Figure 2.3. Morphology of 3D-Gn* (a-d).

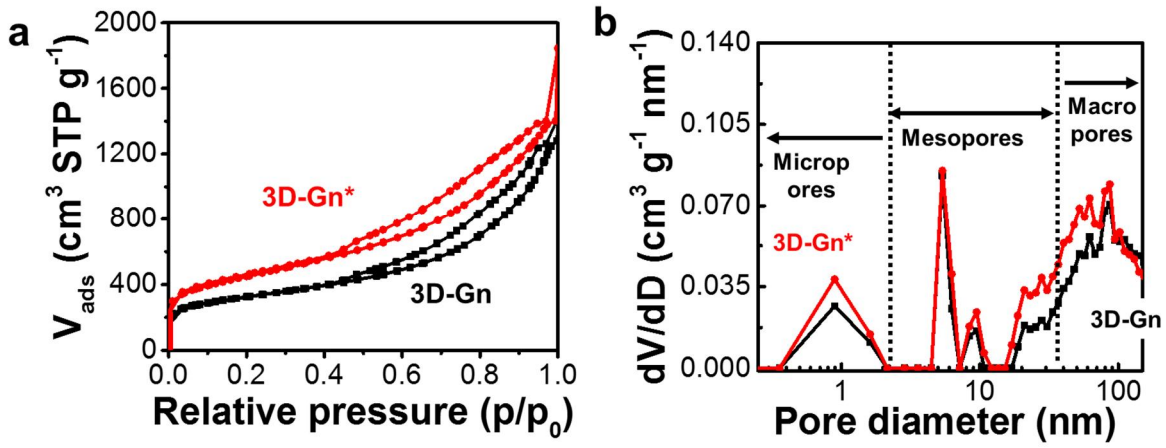

Figure 2.4. Activated 3D-Gn (3D-Gn*) by CO2 activation. Nitrogen adsorption/desorption isotherms (a). Pore size distribution (b).

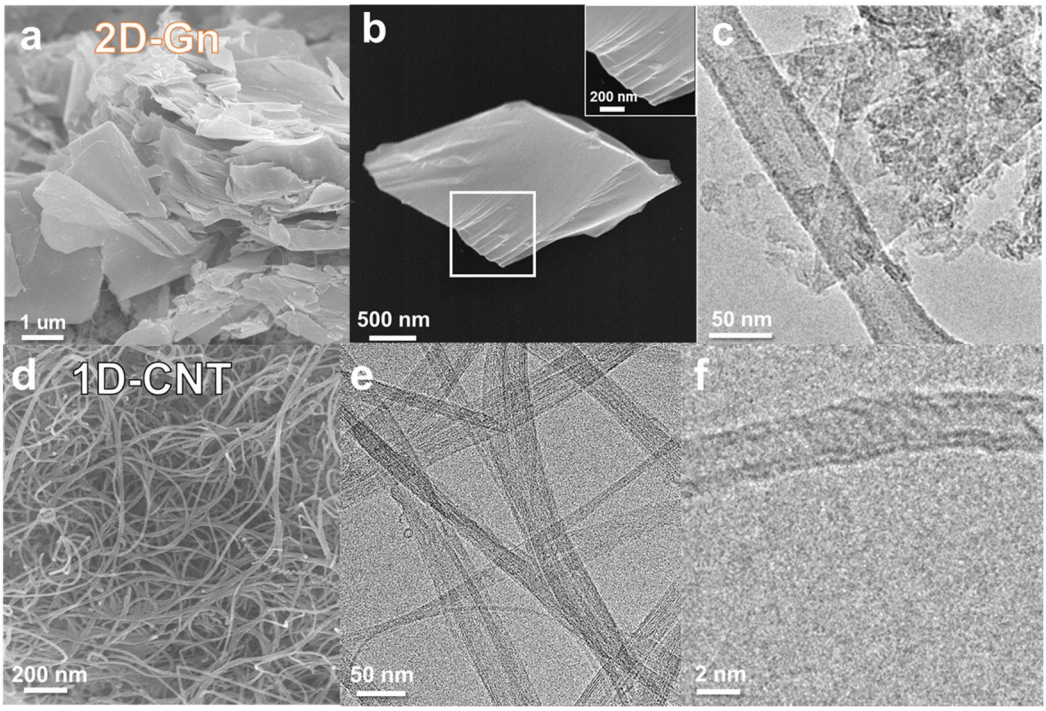

Figure 2.5. Morphology of 2D-Gn (a-c) and 1D-CNT (d-f).

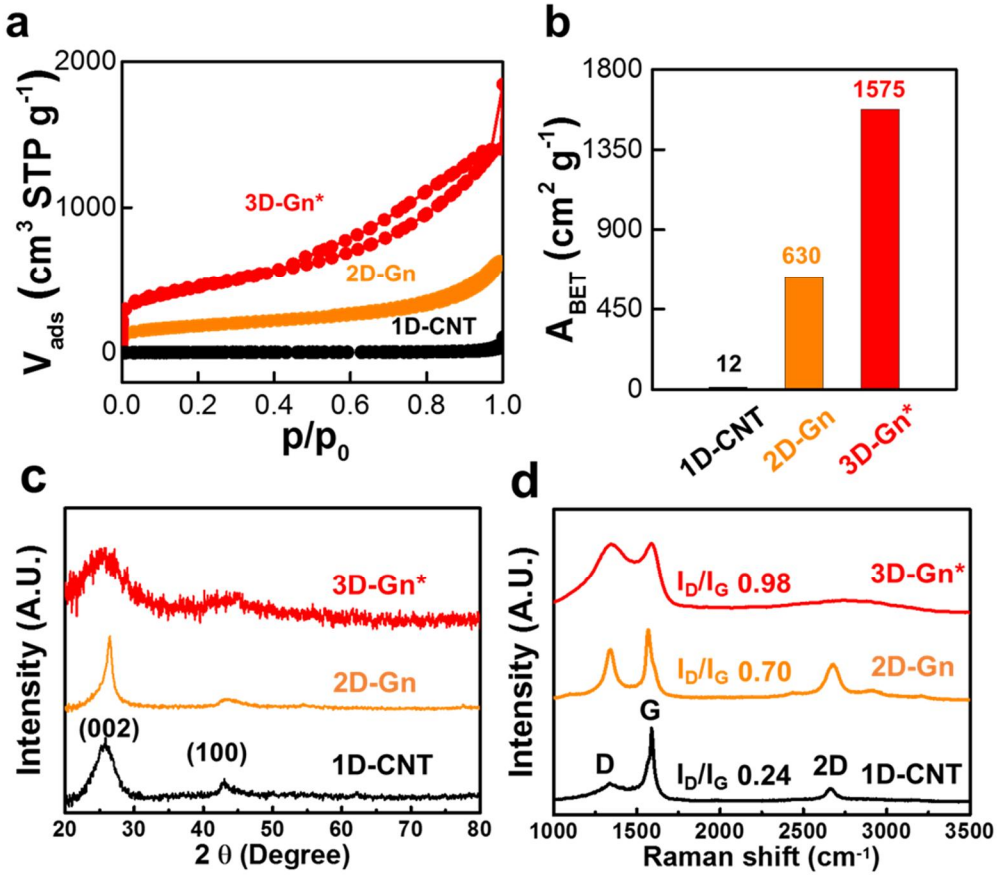

Figure 2.6. Characterization of 3D-Gn*, 2D-Gn and 1D-CNT. (a) Nitrogen adsorption/desorption isotherm. (b) Surface area calculated by Brunauer, Emmett and Teller equation. (c) XRD patterns. (d) Raman spectra.

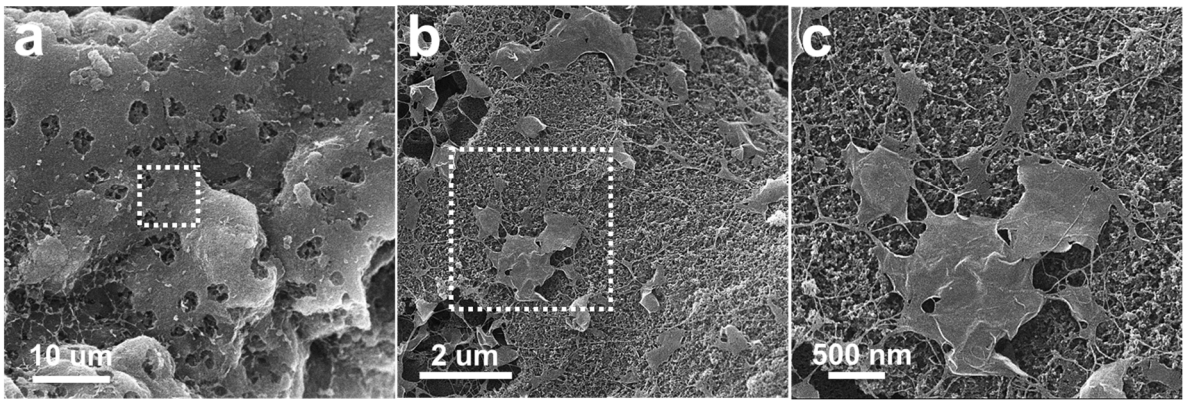

Figure 2.7. Morphology of (3*+2+1)D carbon composites

The (3*+2+1)D composite electrode was designed to fully utilize the surface area by compensating the contact resistance between 3D-Gn*s and between 3D-Gn* and 1D-CNT. The 1D-CNT was used as the main conduction path for the (3*+2+1)D composites based on high electrical conductivity. And it was confirmed that only 1D-CNT on polymer substrate exhibited a high conductivity (295 S cm^{-1}). When the carbon composites were made using 3D-Gn* and 1D-CNT without 2D-Gn, the conductivity seriously decreased to 37 S cm^{-1} and it is considered that the contact resistance was increased. When the carbon composite including the 2D-Gn is made, the conductivity increased again (93 S cm^{-1}) **(Fig. 2.8)**. Therefore, it was predicted that the introduction of 2D-Gn would compensation the contact resistance by widening electron channels between two domains.

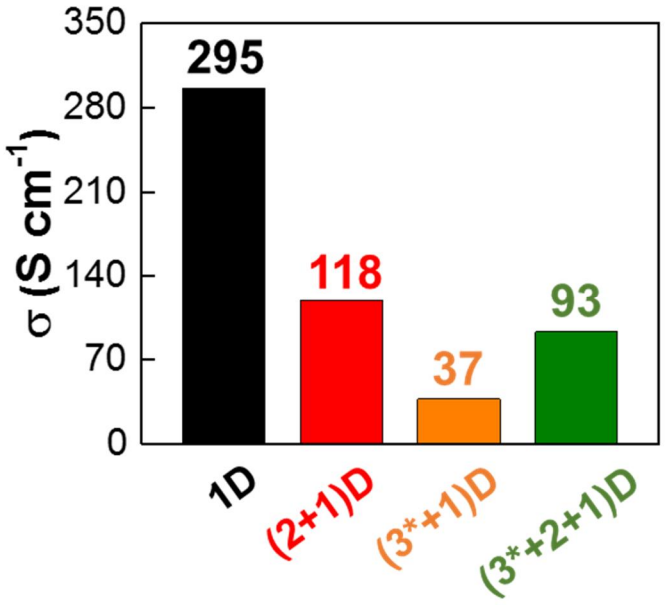

Figure 2.8. Electric conductivities (σ) measured by 4-point probe method of 1D, (2+1)D, (3*+1)D and (3*+2+1)D carbon composites.

2.3.2 Capacitance

The (3*+2+1) D composites as both electrodes were tested in coin-type cells of symmetric EDLCs. And 1M tetraethylammonium tetrafluoroborate in acetonitrile was used as the electrolyte of EDLCs. To estimate contribution of each component in overall capacitance, (3*+2+1)D, (2+1)D and (3*+1)D were measured **(Fig. 2.9)**. Then, the capacitances of 3*D and 2D were calculated by : 3*D = (3*+1)D – 1D ; (2+1)D - 1D. The calculated capacitances of 3D-Gn*(or 3D*), 2D-Gn and 1D-CNT were 87 Fg_{3D}^{-1}, $5Fg_{2D}^{-1}$, and $17g_{1D}^{-1}$, respectively. On the other hand, the capacitance of 3*D in (3*+2+1)D was calculated by (3*+2+1)D-2D-1D : 124 F g_{3D}^{-1}. This value is higher than that of (3*+1)D. As the introduction of 2D-Gn reduced the contact resistance between 3D-Gn*s, the whole surface area of 3D-Gn could be utilized, and it is estimated that the capacitance of 3D* in (3*+2+1)D increased.

The (3*+2+1)D-based EDLC had a higher capacitance when compared to (3*+1)D-based EDLC from cyclic voltammograms at 20mV s^{-1} ; 190 F g^{-1} from (3*+2+1)D versus 130 F g^{-1} from (3*+1)D and from galvanostatic discharge at 0.5 A g^{-1} ; 250 F g^{-1} from (3*+2+1)D versus 150 F g^{-1} from (3*+1)D. **(Fig. 2.10)**. The capacity retention during repetition of charging/discharging at 10A g^{-1} was 98 % for (3*+2+1)D and 97 % for (3*+1)D at 10,000 cycles; 82 % for (3*+2+1)D and 73 % for (3*+1)D at 100,000 cycles (**Figure 2.9**).

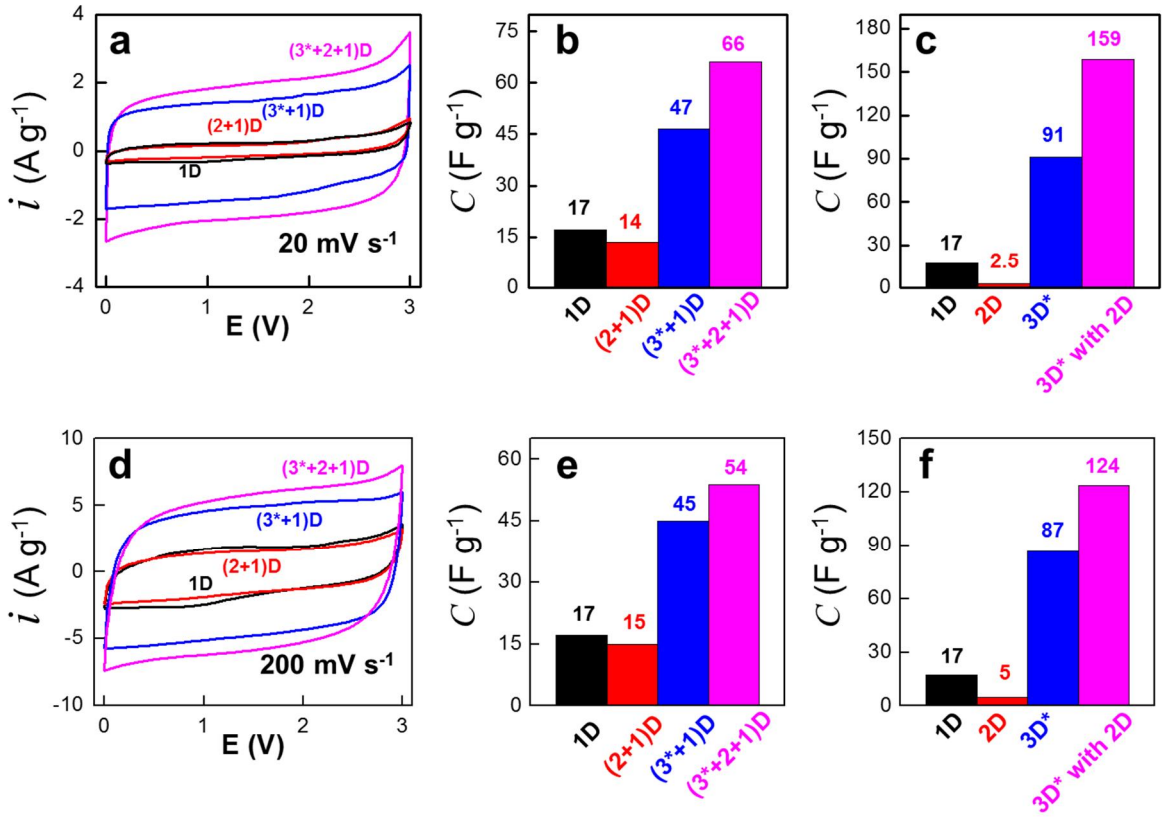

Figure 2.9. Capacitances. Cyclic voltammograms at 20 mV s^{-1} (**a**) and 200 mV s^{-1} (**d**). Capacitance calculated from **a** and **c**. Each capacitance of carbon composites calculated from **b** and **d**.

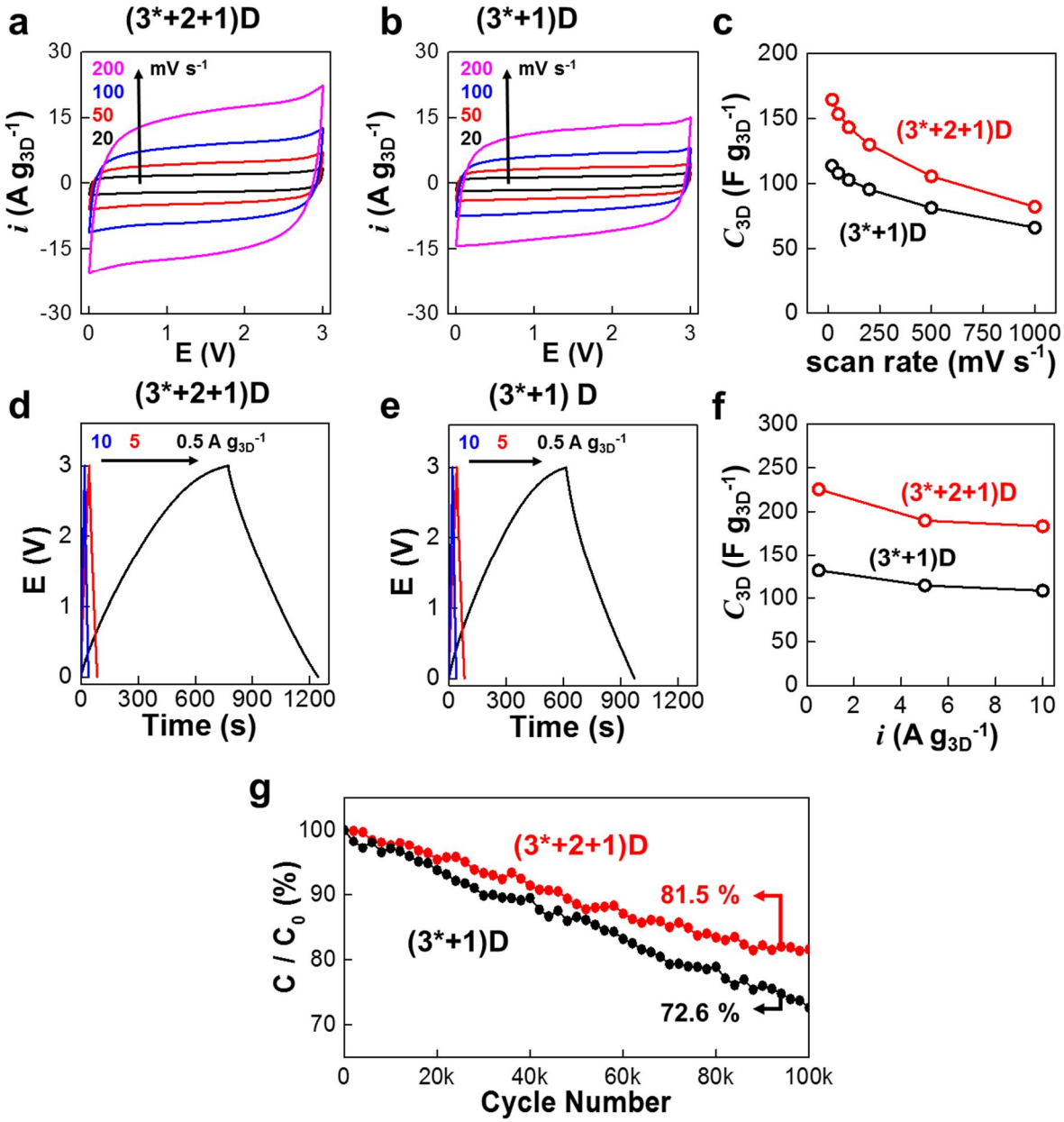

Figure 2.10. Capacitance of (3*+2+1)D versus (3*+1)D. Cyclic voltammograms. (a and b), Capacitance according to scan rates.(c) Galvanostatic charge/discharge profile. (d and e) Capacitance according to current densities (f). Capacitance retention along repeated 100,000 cycles of charging and discharging at 10 A g^{-1}. (g) Energy density versus power density in Ragone plot.

2.3.3 Electrochemical analysis

The increased capacitance of 3D-Gn* with 2D-Gn and 1D-CNT was confirmed by mass change **(Fig. 2.11)**. As the potential is swept away at the point of zero charge, the ions accumulate in the electric double layer of the electrode surface. Thus, the capacitance is directly related to the change in mass of the electrode during the potential sweep. Carbon mixture deposited on gold-plated quartz crystal resonators and it used as working electrode with the same electrolyte used in the EDLCs. Potential was swept from the rest potential found around -0.1 V Ag/Ag^+ (V versus Ag/Ag^+) to – 0.6V Ag/Ag+. The frequency and current of the resonator are measured during a potential scan. Loss of frequency means mass increase. In this EDLC system, tetraethylammonium ion (TEA^+) formed an electric double layer during negative potential sweep and it caused a mass increase. After the backward potential scan, the frequency get the initial value at the rest potential. The frequency change of (3*+2+1)D was about -50 Hz at -0.6 V Ag/Ag^+. It is more negative than that of (3*+1)D. It means the large mass change occurs at (3*+2+1)D. Electrochemically available surface area(A_{EQCM}) was calculated from the mass differences of the adsorbed ions under the assumption that a monolayer of spherical TEA^+ covers a whole surface area of active materials. The A_{EQCM} of 3D-Gn* with 2D-Gn was more than two times that of 3D-Gn* without 2D-Gn. It can explain that the presence of 2D-Gn could help utilize the surface area of 3D-Gn* and it showed improved capacitance.

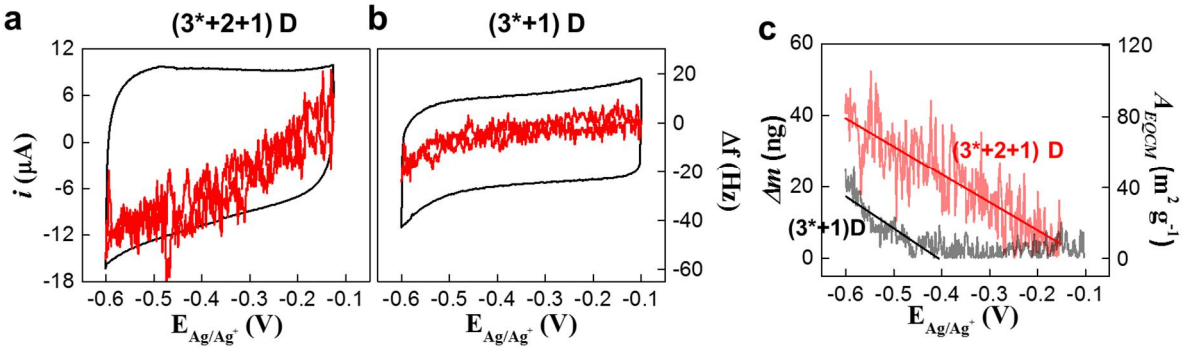

Figure 2.11. Electric double layer formation investigated by electrochemical quartz microbalance. Frequency changes (Δf) during voltage sweep at 10 mVs^{-1} (a and b). Mass differences (Δm) between (3*+2+1)D and (2+1)D or between (3*+1)D and 1D (c).

The porous structure of the multi-dimensional carbon composite was analyzed in terms of ions responsible for the formation of electric double layer. The impedance spectrum of the capacitive

process at the porous electrode deviated significantly from the impedance spectrum of the ideal capacitor at the Nyquist plot[51-53]. Two frequency dispersions appeared and the first frequency dispersion was related to the pore length. Since the ions did not reach the bottom of the pores at high frequency, the overall surface area of the pores was difficult to know. The classical de Levie model described in-a-pore distribution in which an ideal capacitive vertical line was shifted from a high frequency to a 45 degree phase angle line[54]. The second frequency dispersion is due to the distribution of pore sizes. Depending on the size of the pores, the penetration length of the ions was different even at the same frequency. Ions detected surfaces at deeper locations of larger pores. Instead of the vertical line (phase angle = 90 degrees), a constant-phase-angle line (45 degree < phase angle < 90 degree) was obtained at low frequencies. The transmission line model with pore size distribution (TLM-PSD) proposed by Song et al. describes this pore-sized distribution dispersion as well as the in-a-pore dispersion[51-53]. Therefore, the impedance spectrum of the multi-dimensional carbon composite electrode was fitted to TLM-PSD to obtain pore parameters. And the average pore lengths of (3*+2+1)D, and (3*+1)D were 200 μm, and 130 μm, respectively. Therefore, it can be seen that 2D-Gn helps to reduce the contact resistance between 3D-Gn*s and to use the whole surface area of 3D-Gn*. **(Fig 2.12)**

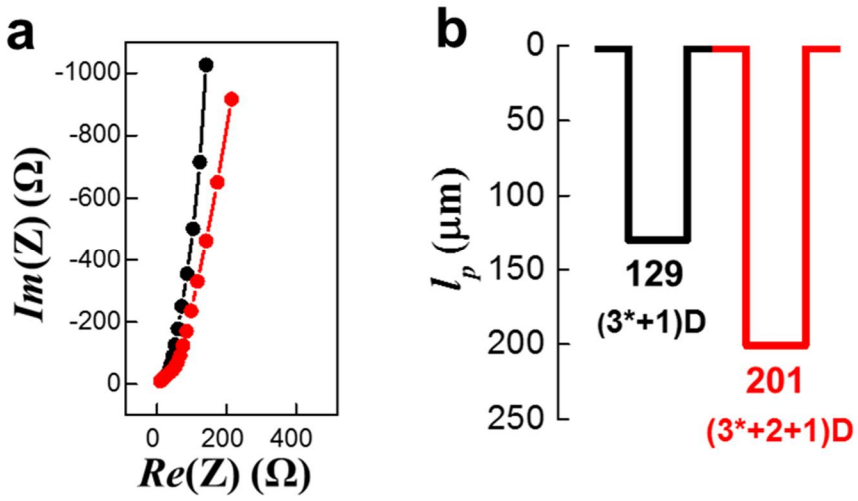

Figure 2.12. Electrochemical impedance spectra (**a**). Experimental data were fitted by transmission line model with pore size distribution (TLM-PSD). Pore length of 3D-Gn* in (3*+2+1)D and (3*+1)D calculated from TLM-PSD (**b**).

2.3.4 Flexibility

From the viewpoint of cohesion and/or adhesion strengths, mass change of the (3*+2+1)D and (3*+1)D composite electrode on the flexible substrate and 3D*|Al electrode was examined under repeated crumpling **(Fig. 2.13a)**. As expected, in the case of the carbon composite on the flexible substrates, it was confirmed that the mass reduction was less than that of the 3D*|Al electrode and it did not change even at 1000 times crumpling.

Although no significant mass changes of carbon composite electrode were observed, the physical crack occurred due to the accumulation of repetitive external stresses. In the absence of 2D-Gn, severe cracks which could cause discontinuity of carbon mass were found at the 500^{th} and 1000^{th} crumpling. However, in the presence of 2D-Gn, mass continuity was maintained. The mechanical durability of the flexible substrate prevented a large increase in resistance under the repeated stress conditions The increased resistance values of (3*+2+1)D and (3*+1)D did not significantly affect the electrical defects. There were insignificant resistance increase measured for the (3*+2+1)D having no mass change an no discontinuity evolution. On the other hand. the 2D-absent (3*+1)D showed a not-serious-but-significant increase of resistance due to the microscopic cracks leading to mass discontinuity: resistance increase = 27 % for (3*+1)D versus 10 % for (3*+2+1)D **(Fig.2.13 b-h)**.

Therefore, the mechanically durable and electrically durable properties of multi-dimensional carbon composite electrodes did not significantly change in the cyclic voltammogram of an EDLC cell based on (3*+2+1)D even when bent and folded. there were no differences of galvanostatic cyclability between the unfolded cell, the 90-degree-bent cell and the completely folded cell during 10,000 cycles of repeated charge and discharge. And the capacity retention at the 100^{th} cycle and at the $100{,}000^{th}$ cycle in the completely folded EDLC cell based on the (3*+2+1)D composite electrodes showed that 92.4% and 71%, respectively. Also, these results confirmed that a light-emitting diode (LED) was emitted light even after the EDLC was rolled and crumpled, half-folded and twice half-folded **(Fig. 2.14)**.

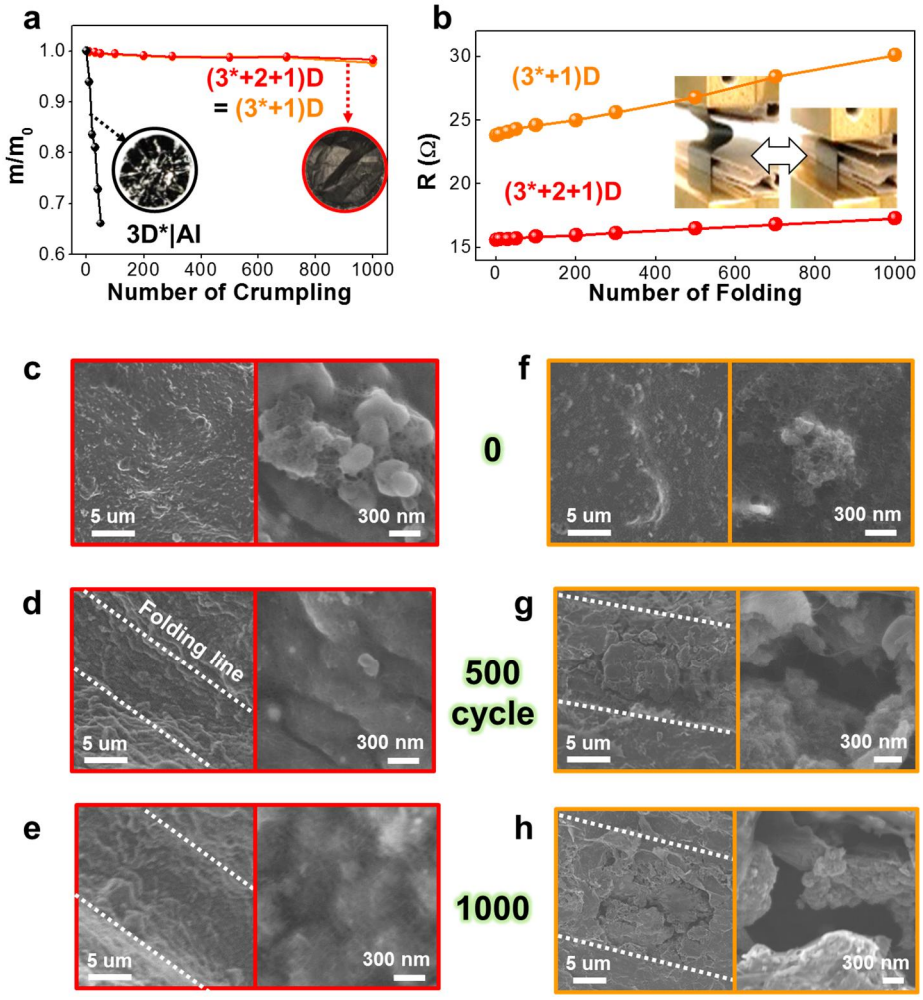

Figure 2.13. Flexibility of (3*+2+1)D or (3*+1)D on polymer substrates vesus 3D*|Al. Mass loss on repeated crumpling (a). Resistance developed along repeated folding (c to h). Top views around folding lines in SEM images at 0, 500 and 1000 times folding: (3*+2+1)D on the left versus (3*+1)right.

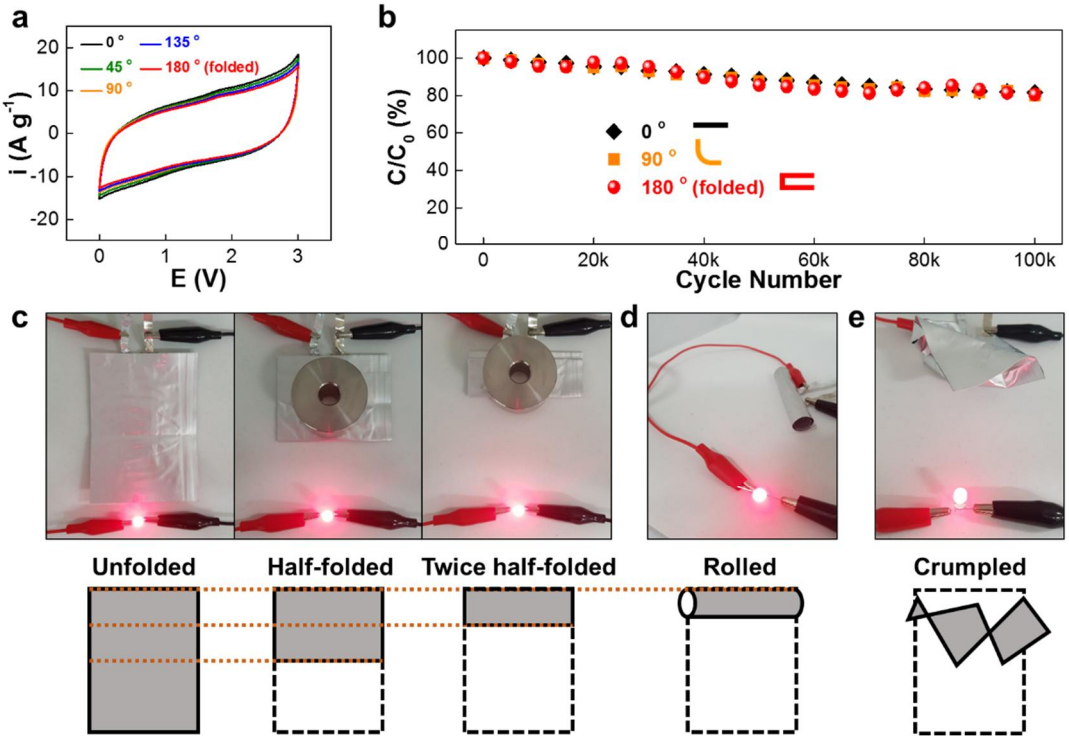

Figure 2.14. Folded supercapacitors. CVs of flexible supercapacitors based on a symmetric (3*+2+1)D electrode configuration on bending at 0º, 90 º and 180 (b-e)

2.4 Conclusion

We successfully fabricated a (3*+2+1)D carbon composite on flexible polymer substrate for flexible EDLC supercapacitors. Each dimensional carbon served as an electron pathway (1D-CNT), compensation of contact resistance (2D-Gn), and capacitive property, and was anchored to the substrate without a binder (1D-CNT). The (3*+2+1)D-based EDLCs were mechanically durable against bending, folding rolling and even crumpling without sacrificing energy densities. This work shows that architectural design of electrodes is important to fully utilize intrinsic capacitance or capacity of active materials and to make electrodes durable against mechanical stress.

References.

1. Winter, M., Brodd, R.j., What are batteries, Fuel cells, and Supercapacitors?. *Chem. Rev.*, **2004**, *104* (10), 4245–4270.

2. P. Simon, Y. Gogotsi, Materials for electrochemical capacitors. *Nat. Mater.*, **2008**, 7, 845-854.

3. M.D. Stoller, S. Park, Y. Zhu, J. An and R.S. Rouf, Graphene-Based Ultracapacitors, *Nano lett.*, **2008**, 8, 3498.

4. H.P. Wu, D.W. He, Y.S. Wang, M. Fu, Z.L. Liu, J.G. Wang and H.T. Wang, IEEE, **2010**, 465.

5. Sharma P, Bhatti T, A review on electrochemical double-layer capacitors. *Energy Convers Manag* **2010**, 51(12), 2901–12

6. Stoller, M.D., Park,S., Zhu,Y., An,J.,and Ruoff,R.S., Graphene-based ultracapacitors, *Nano Lett*., **2008**, 8(10), 3498–3502.

7. A. Schneuwly and R. Gallay, Properties and application of supercapacitors From the state of the art to future trends, *PCIM*, **2000**, 1.

8. Miller JR, Simon P., Materials science: electrochemical capacitors for energy management, *Science*, **2008**, 321, 651-2.

9. K. Jost, G. Dion, Y.Gogotsi, Textile energy storage in perspective, *J. Mater. Chem. A*., 2014, **2**, 10776.

10. Y. Gogotsi, Materials science: Energy storage wrapped up, *Nature,* **2014**, 509, 7502.

11. Dai L, Chang DW, Baek JB et al., Carbon materials for advanced energy conversion and storage, *Small*, **2012**, 8, 1130-66.

12 Q. Li, Z. Li, L. Lin, X. Wang, Y. Wang, C. Zhang and H. Wang, Facile synthesis of activated carbon/carbon nanotubes compound for supercapacitor application*, Chem. Eng. J.*, **2010**, 156, 500.

13. H. Yang, S. Kannappan, A.S. Pandian, J.H Jang, Y.S. Lee and W. Lu, Graphene supercapacitor with both high power and energy density, *Nanotechnology*, **2017**, 28, 445401.

14. Z. Bo, Z. Wen, H. Kim, G. Lu, K. Yu and J. Chen, One-step fabrication and capacitive behavior of electrochemical double layer capacitor electrodes using vertically-oriented graphene directly grown on metal, *Carbon*, **2012**, 50, 4379.

15. A.P. Singh, P. B. Karandikar and N.K. Tiwari, Effect of electrode shape on the parameters of supercapacitor, IEEE, **2015**, 669-73.

16. Y Wang, Z Shi, Y Huang, Y Ma, C Wang, M Chen, Y Chen, Supercapacitor Devices Based on Graphene Materials, *J. Phys. Chem. C*, **2009**, 113(30), 13103-13107.

17. Q. Cheng, J. Tang, J. Ma, H. Zhang, N. Shinya and L.C. Qin, Graphene and carbon nanotube composite electrodes for supercapacitors with ultra-high energy density. *Phys. Chem. Chem. Phys*, **2011**, 13, 17615.

18. P. Tamilarasan, A.K. Mishra and S. Ramaprabhu, Sturdy of removal of azo dye by functionalized multi walled carbon nanotubes, *Chem. Eng. J.*, **2011**, 162, 1026-1034.

19. C. Du and N. Pan, Carbon Nanotube-Based Supercapacitors, *Nanotech. Law & Business*, **2007**, 4, 569.

20. A.G. Pandolfo and A.F. Hollenkamp, Carbon properties and their role in supercapacitors, *J. Power Sources*, **2006**, 157, 11.

21. M.S. Halper and J. C.Ellenbogen, Supercapacitors: A brief overview, *Mitre Nanosystems Group*, **2006**.

22. D.C. Marcano, D.V. Kosynkin, J.M. Berlin, A. Sinitskii, Z. Sun, A. Slesarev, L.B. Alemany, W. Lu and J.M. Tour, Improved synthesis of graphene oxide, *ACS nano*, **2010**, 4, 4806.

23. J.L. Xia, F. Chen, J.H. Li, N.J. Tao, Measurement of the quantum capacitance of graphene, *Nat Nanotechnol.*, **2009**, 4, 505-509.

24. C. Liu, Z. Yu, D. Neff, A. Zhamu and B.Z Jang, Graphene-based supercapacitors with an ultrahigh energy density, *Nano lett.*, **2010**, 10, 4863.

25. R. Ramachandran, V. Mani, S.M. Chen, R. Saraswathi and B.S. Lou, Recent trends in graphene based electrode materials for energy storage devices and sensors applications, *Int. J. Electrochem. Sci.*, **2013,** 8, 11680.

26. R. Ramachandran, M. Saranya, V. Velmurugan,B.P.C. Raghupathy, S.K. Jeong and A.N. Grace, Effect of reducing agent of graphene synthesis and its influence on charge storage towards supercapacitor applications, Applied Energy, **2015**, 153, 22-31.

27. T. Kuilla, S. Bhadra, D. Yao, N.H. Kim, S. Bose and J.H. Lee, Recent advances in graphene-based polymer composites, *Progress Polymer Sci.*, **2010,** 35, 1350.

28. Yang Z, Ren J and Zhang Z et al., Recent advancement of nanostructured carbon for energy applications. *Chem Rev*, **2015**, 115, 5159-223.

29. Liu L, Yu Yan C, Li K, Zheng Z., Wearable energy-dense and power-dense supercapacitor yarns enabled by scalable graphene-metallic texile composite eletrodes. *Nature Commun*, **2015**, 6, 7260.

30. Chmiola J, Yushin G and Gogotsi Y et al., Anomalous increase in carbon capacitance at pore size less than 1 nanometer, *Science*, **2006**, 313, 1760-3.

31. Simon P and Gogotsi Y., Materials for electrochemical capacitors, *Nat Mater*, **2008**, 7, 845-54.

32. Li W, Liu J and Zhao D., Mesoporous materials for energy conversion and storage devices, *Nat Rev Mater*, **2016**, 1, 16023.

33. Xia K, Gao Q and Jiang J et al., Hierarchical porous carbons with controlled micropores and mesopores for supercapacitors electrode materials, *Carbon*, **2008**, 46, 1718-26.

34. Hwang, C., Song, W. J., Han, J. G., Bae, S., Song, G., Choi, N. S., Park, S. and Song, H. K., Foldable Electrode Architectures Based on Silver-Nanowire-Wound or Carbon-Nanotube-Webbed

Micrometer-Scale Fibers of Polyethylene Terephthalate Mats for Flexible Lithium-Ion Batteries., *Adv. Mater.,* **2018**, 30, 1705445.

35. Kwon, Y. H., Park, J. J., Housel, L. M., Minnici, K., Zhang, G., Lee, S. R., Lee, S. W., Chen, Z., Noda, S., Takeuchi, E. S., Takeuchi, K. J., Marschilok, A. C., and Reichmanis, E., Carbon Nanotube Web with Carboxylated Polythiophene "Assist" for High-Performance Battery Electrodes. *ACS Nano* **2018,** *12*, 3126-3139.

36. Ko, Y., Kwon, M., Bae, W. K., Lee, B., Lee, S. W., Cho, J., Flexible Supercapacitor Electrodes Based on Real Metal-Like Cellulose Papers. *Nat. Commun.* **2017,** *8*, 536.

37. Li, X., Tang, Y., Song, J., Yang, W., Wang, M., Zhu, C., Zhao, W., Zheng, J., Lin, Y., Self-Supporting Activated Carbon/Carbon Nanotube/Reduced Graphene Oxide Flexible Electrode for High Performance Supercapacitor, *Carbon,* **2018,** 129, 236-244.

38. Zhu, Y.-H., Yang, X., Bao, D., Bie, X.-F., Sun, T., Wang, S., Jiang, Y.-S., Zhang, X.-B., Yan, J.-M., Jiang, Q., High-Energy-Density Flexible Potassium-Ion Battery Based on Patterned Electrodes. *Joule* **2018,** *2*, 736-746.

39. Wang, H.-G., Li, W., Liu, D.-P., Feng, X.-L., Wang, J., Yang, X.-Y., Zhang, X.-B., Zhu, Y., Zhang, Y., Flexible Electrodes for Sodium-Ion Batteries: Recent Progress and Perspectives. *Adv. Mater.* **2017,** *29*, 1703012.

40. Zhu, Y.-H., Yuan, S., Bao, D., Yin, Y.-B., Zhong, H.-X., Zhang, X.-B., Yan, J.-M., Jiang, Q., Decorating Waste Cloth Via Industrial Wastewater for Tube-Type Flexible and Wearable Sodium-Ion Batteries. *Adv. Mater.* **2017,** *29*, 1603719.

41. Yin, Y.-B., Xu, J.-J., Liu, Q.-C., Zhang, X.-B., Macroporous Interconnected Hollow Carbon Nanofibers Inspired by Golden-Toad Eggs toward a Binder-Free, High-Rate, and Flexible Electrode. *Adv. Mater.* **2016,** *28*, 7494-7500.

42. Shao, Y., El-Kady, M. F., Wang, L. J., Zhang, Q., Li, Y., Wang, H., Mousavi, M. F., Kaner, R. B., Graphene-Based Materials for Flexible Supercapacitors. *Chem. Soc. Rev.* **2015,** *44*, 3639-3665.

43. Liu, W., Chen, Z., Zhou, G., Sun, Y., Lee, H. R., Liu, C., Yao, H., Bao, Z., Cui, Y., 3d Porous Sponge-Inspired Electrode for Stretchable Lithium-Ion Batteries. *Adv. Mater.* **2016,** *28*, 3578-3583.

44. Lu, H., Hagberg, J., Lindbergh, G., Cornell, A., $Li_4Ti_5O_{12}$ Flexible, Lightweight Electrodes Based on Cellulose Nanofibrils as Binder and Carbon Fibers as Current Collectors for Li-Ion Batteries. *Nano Energy* **2017,** *39*, 140-150.

45. Gwon, H., Kim, H.-S., Lee, K. U., Seo, D.-H., Park, Y. C., Lee, Y.-S., Ahn, B. T., Kang, K., Flexible Energy Storage Devices Based on Graphene Paper. *Energy Environ. Sci.* **2011,** *4*, 1277-1283.

46. Choi, K.-H., Yoo, J., Lee, C. K., Lee, S.-Y., All-Inkjet-Printed, Solid-State Flexible Supercapacitors on Paper. *Energy Environ. Sci.* **2016,** *9*, 2812-2821.

47. Cho, S.-J., Choi, K.-H., Yoo, J.-T., Kim, J.-H., Lee, Y.-H., Chun, S.-J., Park, S.-B., Choi, D.-H., Wu, Q., Lee, S.-Y., Lee, S.-Y., Hetero-Nanonet Rechargeable Paper Batteries: Toward Ultrahigh Energy Density and Origami Foldability. *Adv. Funct. Mater.* **2015,** *25*, 6029-6040.

48. Yang, X., Cheng, C., Wang, Y., Qiu, L., Li, D., Liquid-Mediated Dense Integration of Graphene Materials for Compact Capacitive Energy Storage. *Science* **2013,** *341*, 534-537.

49. Ramadoss, A., Yoon, K.-Y., Kwak, M.-J., Kim, S.-I., Ryu, S.-T., Jang, J.-H., Fully Flexible, Lightweight, High Performance All-Solid-State Supercapacitor Based on 3-Dimensional-Graphene/Graphite-Paper. *J. Power Sources* **2017,** *337*, 159-165.

50. Yoon, J.-C., Lee, J.-S., Kim, S.-I., Kim, K.-H., Jang, J.-H., Three-Dimensional Graphene Nano-Networks with High Quality and Mass Production Capability via Precursor-Assisted Chemical Vapor Deposition. *Sci. Rep.* **2013,** *3*, 1788.

51. Kwak, M.-J., Ramadoss, A., Yoon, K.-Y., Park, J., Thiyagarajan, P., Jang, J.-H., Single-Step Synthesis of N-Doped Three-Dimensional Graphitic Foams for High-Performance Supercapacitors. *ACS Sustainable Chem. Eng.* **2017,** *5*, 6950-6957

52. Song, H.-K., Sung, J.-H., Jung, Y.-H., Lee, K.-H., Dao, L. H., Kim, M.-H., Kim, H.-N., Electrochemical Porosimetry. *J. Electrochem. Soc.* **2004,** *151*, E102-E109.

53. Song, H.-K., Hwang, H.-Y., Lee, K.-H., Dao, L. H., The Effect of Pore Size Distribution on the Frequency Dispersion of Porous Electrodes. *Electrochim. Acta* **2000,** *45*, 2241-2257.

54. Song, H.-K., Jung, Y.-H., Lee, K.-H., Dao, L. H., Electrochemical Impedance Spectroscopy of Porous Electrodes: The Effect of Pore Size Distribution. *Electrochim. Acta* **1999,** *44*, 3513-3519.

55. De Levie, R., Electrochemical Response of Porous and Rough Electrodes. *Advances in electrochemistry and electrochemical engineering* **1967,** *6*, 329-397.

56. Y Wang, Z Shi, Y Huang, Y Ma, C Wang, M Chen, Y Chen, Supercapacitor Devices Based on Graphene Materials, J. Phys. Chem. C **2009**, 113(30), 13103-13107.

57. Mosch, H. L., Akintola, O., Plass, W., Hoppener, S., Schubert, U. S., Ignaszak, A., Specific Surface Versus Electrochemically Active Area of the Carbon/Polypyrrole Capacitor: Correlation of Ion Dynamics Studied by an Electrochemical Quartz Crystal Microbalance with Bet Surface. *Langmuir* **2016,** *32*, 4440-4449.

58. Lam, V. W. S., Kannangara, D. C. W., Alfantazi, A., Gyenge, E. L., Electrochemical Quartz Crystal Microbalance Study of Borohydride Electro-Oxidation on Pt: The Effect of Borohydride Concentration and Thiourea Adsorption. *J. Phys. Chem. C* **2011,** *115*, 2727-2737.